Long-Term Variations of Cosmic Rays and Terrestrial Environment

Ilya G. Usoskin
Sodankylä Geophys. Observatory (Oulu unit), University of Oulu, Finland
Ilya.Usoskin@oulu.fi

Abstract

This rapporteur talk aims to review scientific contributions to the following sessions of the 28^{th} International Cosmic Ray Conference (August 2003, Tsukuba, Japan): SH 3.4 "Long-term variations," SH 3.5 "Long-term variation of cosmic rays studied by cosmogenic nuclides," SH 3.6 "Terrestrial effects and cosmogenic nuclides" and partly SH 1.5 "Instrumentation and new projects." Most important results are discussed in the line of long-term cosmic ray variations and terrestrial effects.

1. Introduction

Many interesting contributions have been presented at the 28th ICRC about long-term variations of cosmic rays and terrestrial environment (sessions SH 3.4–SH 3.6 and partly SH 1.5), and it is impossible to cover all of them in this brief review. The selection is subjective, and the primary attention is given to new experimental results and their interpretation. Some statistics of the presented papers and their topical subdivision is summarized Table 1. Although the dispersion of individual paper's topics is quite broad, they generally fit into two main directions, long-term cosmic ray variations and the terrestrial environment. References to the 28th ICRC contribution papers are given using the Session and page numbers in the ICRC Proceeding volumes.

2. Cosmogenic proxies of cosmic rays

In nuclear collisions of energetic cosmic rays with targets in the Earth's atmosphere, numerous secondaries are produced. Some of them are radioactive isotopes and have no other natural sources but cosmic rays. After production and complicated transport in the atmosphere, such cosmogenic isotopes can be stored in various natural archives. Their content in the archive is measured nowadays to estimate the cosmic ray flux in the past. The main advantage of this method is its

pp. 205–228

Table 1. Statistics of reviewed papers.

Long-term cosmic ray modulation	13 (baker's dozen)
Cosmogenic isotopes	13 (baker's dozen)
Terrestrial effects of cosmic rays	13 (baker's dozen)
Transport in the Earth's magnetosphere and atmosphere	13 (baker's dozen)
Details of CR measurements	4
Miscellaneous	13 (baker's dozen)
Total	69

"off-line" type. Thanks to the Mother Nature, primary archiving of cosmogenic isotopes is done routinely in a similar manner throughout the ages. These archives are measured nowadays in laboratories using modern techniques. If necessary, all measurements can be repeated and improved as has been done for some radiocarbon samples [12]. Such an approach gives quite a homogeneous data series of cosmic rays flux in the past.

2.1. ^{10}Be in polar ice

As a product of nuclear collisions of cosmic rays with atmospheric N and O nuclei, the radioactive isotope ^{10}Be (half-life time $\tau_{1/2} = 1.5 \cdot 10^6$ years) is produced. Then it becomes attached to aerosols and falls down to the surface where it is stored in polar ice (for details see the highlight talk by J. Beer in this volume or [5]). Although local climate (in particular the snow precipitation rate) may affect the concentration of ^{10}Be in ice [5], [3], it is believed that the main factor affecting ^{10}Be content in polar ice is related to variations of the ^{10}Be production rate in the atmosphere due to changes in the cosmic ray flux impinging on the Earth's atmosphere. This is verified by a comparison of two ^{10}Be records from Greenland [5] and Antarctica [3], where the climate conditions are very different. It is still not exactly clear what fraction of the global atmosphere contributes to the ^{10}Be data in polar ice, i.e., whether all this ^{10}Be is produced locally in the polar regions or an atmospheric mixing takes place bringing ^{10}Be produced at middle or low latitudes to polar regions. The effective energy of ^{10}Be production in the atmosphere is between 1.3 GeV/nucleon for local polar production model (Alanko et al. SH 3.3, 3901) and about 2 GeV/nucleon for the global mixing model (McCracken, SH 3.5, 4127; [22]). Time profiles of ^{10}Be series is shown in Fig. 1. for the last millennium. An analysis of these series yields some puzzling features which should be understood in terms of the modulation of cosmic ray flux by solar magnetic activity (McCracken, Beer & McDonald, SH 3.5, 4123; McCracken, SH 3.5, 4127): The intensity of cosmic rays with energy

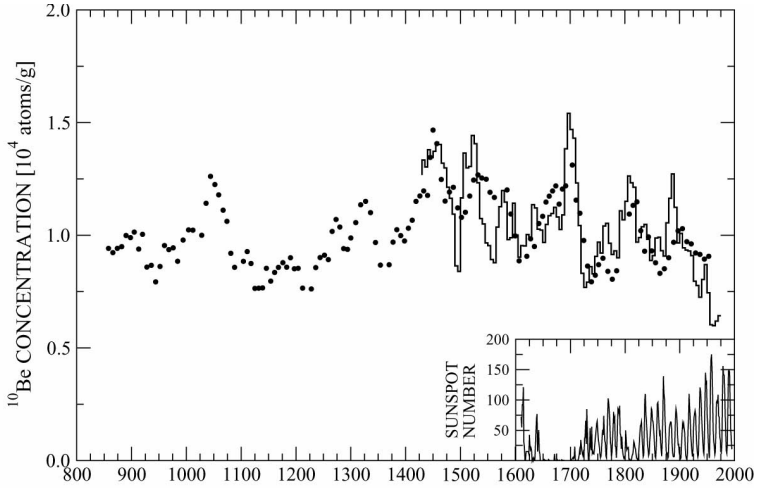

Fig. 1. The 11-year averaged 10 Be data from Dye 3, Greenland (solid line) and 21–24 year averages (dots) from South Pole [3] (from McCracken, Beer & McDonald, SH 3.5, 4123). The observed group sunspot numbers are shown in the incut.

1–2 GeV/nucleon suffered variations by a factor of 2.5 between the times of great minima and present high solar activity; The lowest absolute cosmic ray flux is reached during the last 50 years; A significant modulation of cosmic rays took place during the Maunder minimum (see also [11], [35]) and the sudden decrease of the ^{10}Be level by a factor of 2 within 25 years after that implying a very fast recovery of the heliospheric modulation after the deep minimum; possible 5-y variations during low solar activity found recently by [10]. An interesting relation between the ^{10}Be concentration and the sunspot activity around solar cycle minimum (Fig. 2.) is reported by McCracken, Beer & McDonald (SH 3.4, 4031).

2.2. Radiocarbon ^{14}C in tree rings

Radiocarbon ^{14}C ($\tau_{1/2}$ ≈5730 years) is a product of neutron capture by atmospheric nitrogen (see, e.g., [8]). It is produced initially at the altitude of 10–15 km (Aoki et al., SH 3.5, 4151), then gets oxidized to CO_2 and takes part in the global carbon cycle which includes atmosphere, biosphere and oceans. Transport of radiocarbon in the atmosphere is very complicated and includes exchange between different reservoirs. As a result ^{14}C is globally mixed in the atmosphere. Exchange between these reservoirs attenuates and damps essentially high-frequency (shorter than 100 years) signals but 11- and 22-year cyclicities are still present in the ^{14}C data. Radiocarbon can be absorbed from air by plants during their vegetation and stored there. Usually ^{14}C is measured in tree rings

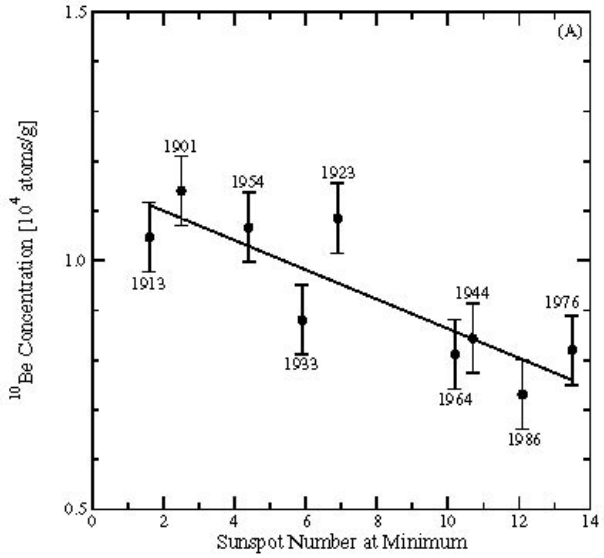

Fig. 2. The ^{10}Be concentrations (weighted average of 3 years about sunspot minimum) versus minimum annual sunspot number (from McCracken, Beer & McDonald, SH 3.4, 4031).

providing thus precise annual resolution of samples. The effective energy of the globally averaged ^{14}C production is about 2.8 Gev/nucleon (Alanko et al., SH 3.3, 3901). The time profile of Δ^{14}C is shown in Fig. 3. after [30]. Great minima of solar activity are clearly seen in the data. One can also notice the steep decrease of the measured ^{14}C since mid-19th century due to burning of large amount of fossil fuel (oil, gas) where all radiocarbon has been decayed through the ages (the so-called Suess effect [32]). This effect as well as atmospheric nuclear tests change the relation between cosmic rays and radiocarbon level in the atmosphere during the last century.

New precise measurements of ^{14}C with annual resolution have been presented by a number of Japanese groups at this conference (H. Sakurai et al., SH 3.5, 4135; Miyahara et al., SH 3.5, 4139; Masuda et al., SH 3.5, 4143) and will be discussed in following sections.

2.3. Short-living ^{7}Be isotope in air

The short-living ($\tau_{1/2}$ =53.3 days) isotope ^{7}Be is produced in the air in a way similar to ^{10}Be. Concentration of ^{7}Be is usually measured directly in air using the 477.6 keV γ-line (Yoshimori et al., SH 3.6, 4217; Sakurai et al., SH 3.6, 4221; Yoshimori, Hirayama & Mori, SH 3.6, 4273). Data of ^{7}Be are used to study the air transport, in particular mixing between troposphere and stratosphere, as

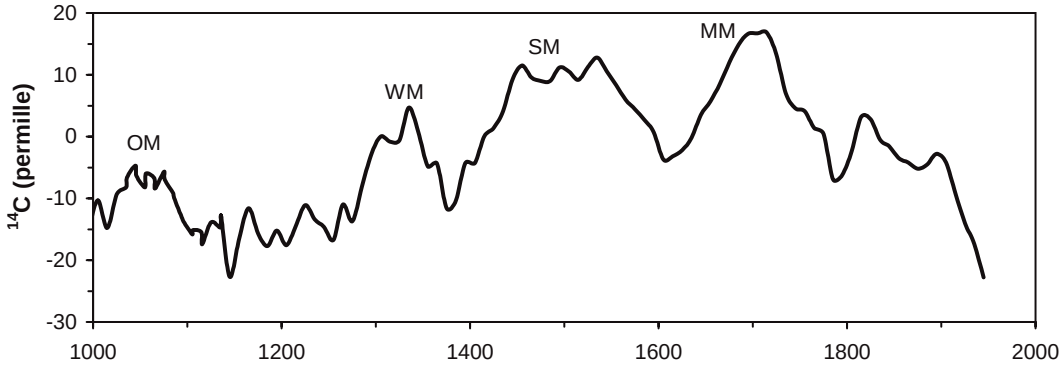

Fig. 3. Time profile of decadal ^{14}C data [30]. Most recent great minima of solar activity are marked: Oort minimum (OM), Wolf minimum (WM), Spörer minimum (SM) and Maunder minimum (MM).

well as the effect of solar energetic particle (SEP) events.

Yoshimori et al. (SH 3.6, 4217) studied seasonal variations of ^{7}Be concentration and found a strong increase during the Spring and a less reliable peak in the Fall (Fig. 4.). Since the bulk of ^{7}Be is produced in stratosphere while the measurements are performed in the troposphere, mixing of air masses between the two regions should result in enhanced concentration of ^{7}Be at the surface level. Accordingly, the found seasonal variations are interpreted by Yoshimori et al. as evidence for tropospheric/stratospheric air mass mixing (e.g., [9],[2]) which takes place in Spring and, probably, also in the Fall.

Sakurai et al. (SH 3.6, 4221) studied the quasi-periodic variations of ^{7}Be data with the synodic solar rotation period (26–27 days). The superposed epoch analysis of 26-day folded data of ^{7}Be, sunspot numbers and cosmic ray flux (measured by neutron monitors) is shown in Fig. 5. The 26-day periodicity is clearly seen in ^{7}Be concentration in phase (with few days delay) with cosmic ray data, in agreement with the cosmogenic nature of these data. However, one can also see a strong 13-day periodicity in phase with sunspot activity which is only marginally present in cosmic ray data. This 13-day periodicity may indicate a solar influence on ^{7}Be production.

2.4. ^{44}Ti in meteorites

Results of ^{44}Ti measurements in meteorites have been presented by Cini Castagnoli et al. (SH 3.4, 4045). During their life, meteorites are subject of continuous bombarding by cosmic rays which can produce radioactive isotopes in their bodies. One such isotope is ^{44}Ti ($\tau_{1/2}$ ≈59 years) which is a product of nuclear interaction of cosmic protons with Fe and Ni. The abundance of ^{44}Ti in

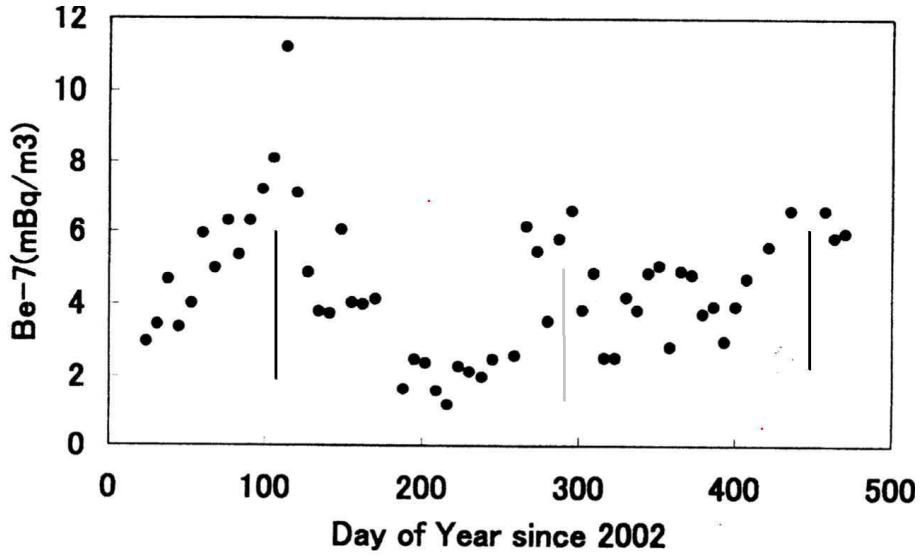

Fig. 4. Seasonal variations of ^{7}Be concentrations since 01.01.2002 (from Yoshimori et al., SH 3.6, 4217). Black and gray lines indicate Spring and Fall peaks, respectively.

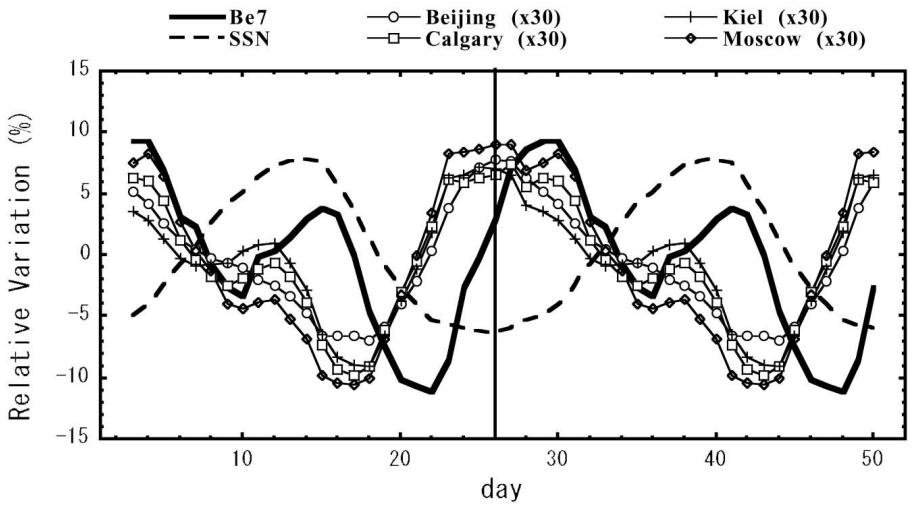

Fig. 5. ^{7}Be concentrations, sunspot numbers, and neutron monitor data (multiplied by a factor of 30) folded with the folding period of 26 days for the each time series (from Sakurai et al., SH 3.6, 4221).

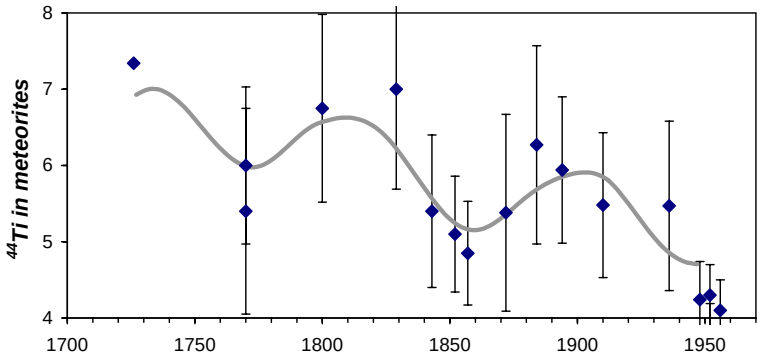

Fig. 6. Measurements of ^{44}Ti in different chondrites together with the long-term trend (after Cini Castagnoli et al., SH 3.4, 4045).

fallen stony meteorites can be measured and gives the intensity of cosmic rays integrated over the meteorite's path. Accordingly, such an approach provides a kind of cosmic ray space probing, i.e., beyond the geomagnetic and atmospheric effects. However, since only the integrated flux can be measured, the time resolution of this method is limited by the isotope's life time.

2.5. Nitrates in polar ice

Another promising proxy is the concentration of nitrates and nitrites (called NO(Y)) in polar ice. Production of NO(Y) in polar atmosphere is greatly enhanced during strong solar energetic particle (SEP) events with the total fluence of protons (>30 MeV) exceeding 10^9 cm^{-2} [38], [13], [23]. After precipitation, NO(Y) can be stored in polar ice where its content can be measured. Accordingly, data on NO(Y) in polar ice is an index of strong SEP events in the past. Shea et al. (SH 3.6, 4225) studied the relations between NO(Y) data from Antarctic ice core and auroras visible in middle latitudes that serves as an index of very strong interplanetary transient phenomenae (Fig. 7.). About 86% (51 out of 59) of the analyzed mid-latitude aurora sightings have clear association with NO(Y) events. This provides further evidence for the solar origin of NO(Y) peaks in polar ice. Moreover, so high correlation of transient and energetic particle phenomenae may indicate that SEP events with largest total fluence are related to CME-driven shocks rather than to solar flares.

Shea et al. (SH 3.6, 4225) reported also a statistically significant season dependence of nitrate peaks. No apparent reason is suggested for such a dependence providing the correct timing of data. Although annual layers can be identified in ice with high accuracy, distribution of samples within the annual ice layer was supposed to be linear. Accordingly, seasonal variations in the local snow

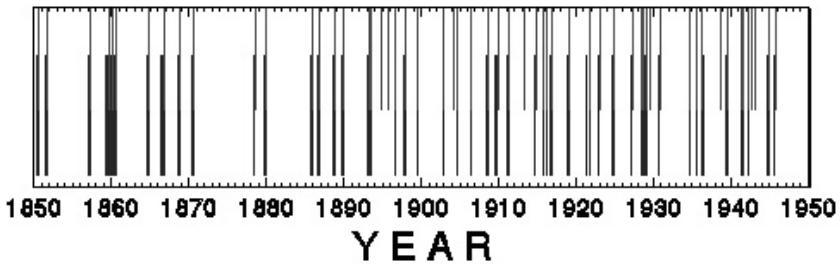

Fig. 7. Association between NO(Y) events from the Antarctic ice core (top) and middle-latitude auroras (bottom) [21], [27] (from Shea et al., SH 3.6, 4225).

deposition may produce a spurious seasonal vawe in NO(Y) data.

3. Great minima of solar activity

Sometimes the regular time evolution of solar activity is intervened by periods of greatly depressed activity called great minima. During such periods the magnetic activity of the Sun is suppressed resulting in enhanced cosmic ray flux at the Earth's orbit. The last great minimum (and the only one covered by direct solar observations) was the famous Maunder minimum during 1645–1715. Other great minima in the past known from cosmogenic isotope data include Spörer minimum in about 1450–1550, Wolf minimum around 12^{th} century, etc. (see Fig. 3.). Such periods are of great interest for solar and stellar astrophysics, and cosmogenic isotopes provides very important (or even the only possible) information on solar/heliospheric parameters during great minima. Some new precise measurements of Δ^{14}C during Maunder and Spörer minima have been reported at the Conference.

3.1. Maunder minimum during 1645–1715

Several direct and indirect data sets have been analyzed covering the Maunder minimum, and the following pattern has been found. The 22-year cyclicity dominated sunspot numbers during the deep minimum in 1645–1700 with the 11-year cycle becoming more pronounced towards the end of the period [35]. A similar pattern is clear in visual aurora occurrence [21], [27] and in NO(Y) data [14]. Radiocarbon ^{14}C data also shows the dominant 22-year periodicity [20], [31], [25]. However, ^{10}Be data in Greenland ice core reveals mainly the 11-year cycle during the Maunder minimum (McCracken, Beer & McDonald, SH 3.5, 4123, see also [6]). This discrepancy should be resolved.

Another problem related to radiocarbon measurements during the Maunder minimum is that the two existing series with annual resolution, by Stuiver

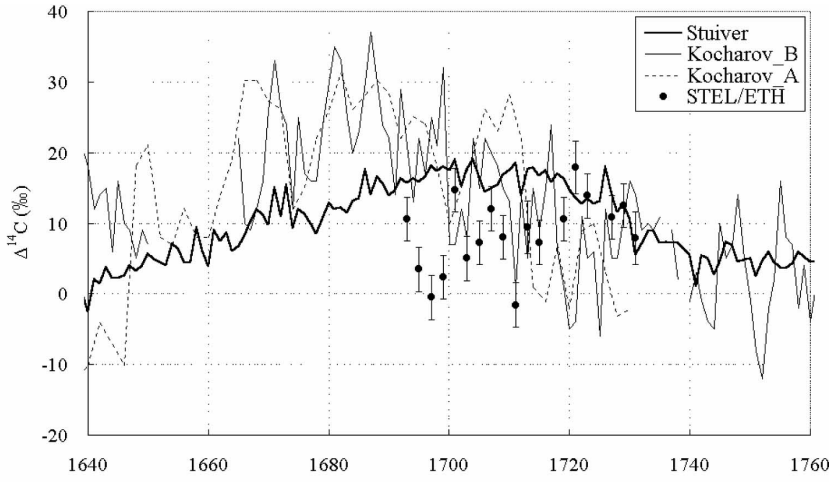

Fig. 8. Time profile of ^{14}C measurements around the Maunder minimum: by Stuiver [30] (thick curve), by Kocharov et al. [20] (thin curves) and by Masuda et al. (SH 3.5, 4143) (dots).

et al. [30] (US East cost) and by Kocharov et al. [20] (Ural region and Western Ukraine), depict different levels of Δ^{14}C variations during the Maunder minimum (Fig. 8.). Although an inter-calibration of the two series has been performed [12], a possible source of the different level of Δ^{14}C variations was still unclear. New independent measurement of Δ^{14}C in a Japanese cedar tree with annual resolution have been presented by Masuda et al. (SH 3.5, 4143) for the late phase of the Maunder minimum (Fig. 8.). While being different from the two other series, the new Japanese series depicts large variations of Δ^{14}C during the second half of the Maunder minimum, similar to Kocharov et al. series. Unfortunately, data for the earlier part of the minimum are not available yet, and we look forward for the whole Maunder minimum covered by the new measurements. This will also clarify the relation between solar cycles during that period.

3.2. Spörer minimum in XV century

The Spörer minimum took place around 1400–1550. It is not well covered by high resolution data, only ^{10}Be data from Greenland were available for this period with nearly annual resolution [5]. At this Conference, the results of new measurements of Δ^{14}C in Japanese cedar tree performed by Miyahara et al. (SH 3.5, 4139) with annual resolution, covering the whole Spörer minimum, have been presented. A preliminary spectral analysis of the radiocarbon data reveals the following main periodicities during the Spörer minimum. The amplitude of 11-year cycle was greatly reduced from about 4 permille outside the minimum to nearly

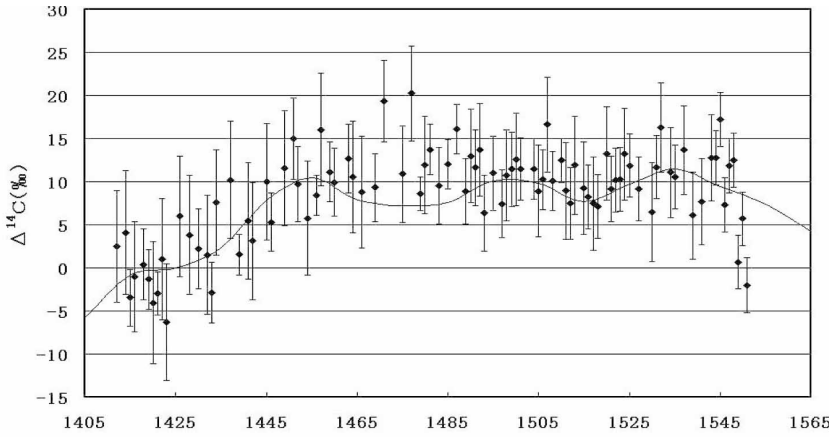

Fig. 9. Time profile of ^{14}C content in Japanese tree rings during the Spörer minimum (from Miyahara et al., SH 3.5, 4139).

zero during the minimum time. The amplitude of the 22-year cycle remained roughly constant (at the level of about 1.2 permille) throughout the 150 years around the Spörer minimum (see Fig. 4 in Miyahara et al., SH 3.5, 4139). Also a significant 7–8-year cycle has been found in ^{14}C data during the minimum. The obtained pattern is very similar to that obtained from the ^{10}Be series during the deep Spörer minimum: strong ≈20-year and 7-year cyclicities with suppression of the 11-year cycle. This pattern agrees very well with a general scenario of the Maunder minimum suggested in [35]: deep suppression of the 11-year cycle on the background of roughly constant 22-year cycle which thus becomes dominant during the deep minimum phase. The fact that the pattern is very similar for the two great minima suggests that they are phenomenae of the same kind and have a similar origin.

4. Sun's shadow

Even though the flux of cosmic rays with TeV energy is not modulated by the solar wind and IMF, they still can serve as probes for solar magnetic fields. These energetic cosmic rays propagate nearly straightly in the heliosphere so that the shadow of the Moon and Sun can be observed in cosmic rays that is used to study angular and energy resolutions of air shower arrays. However, near-solar magnetic fields are able to slightly distort trajectories of CR passing by the Sun and wash out the Sun's shadow during solar magnetic activity maxima (Tibet collaboration, SH 3.4, 4061; Milagro collaboration, SH 3.4, 4065). Fig. 10. shows the Sun's shadow as measured by the Tibet experiment in the 10 TeV energy range. The shadow, which is quite clear with sharp edges during the solar min-

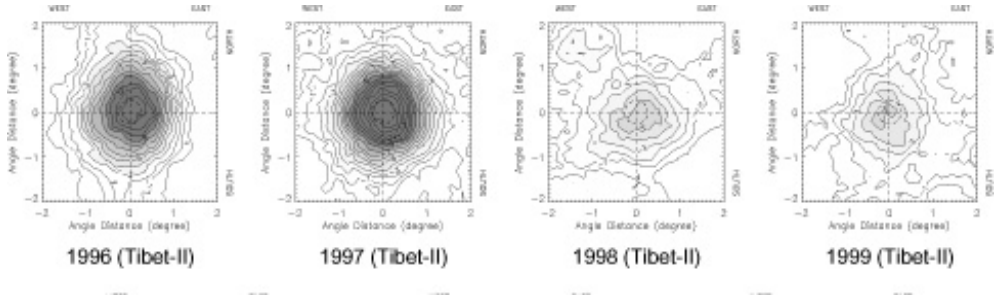

Fig. 10. Yearly variations of the Suns shadow at 10 TeV energy observed by Tibet-II in 1996–1999 (from Amenomori et al. (Tibet collaboration), SH 3.4, 4061).

imum (1996), is washed out around the solar maximum. Accordingly, the Sun's shadow in CR is strongly affected by IMF depicting the solar cycle dependence. A possible south-eastwards displacement of the shadow around maximum was also reported by the Tibet group but not not confirmed by the Milagro group.

5. Environmental monitoring

Several contributions presenting different aspects of environmental monitoring have been presented. The measurements of ^{7}Be in the air have been discussed above. Atmospheric neutrons produced by nuclear interactions of cosmic rays with the atmospheric matter form the most important factor for radiation doses. Zanini et al. (SH 3.6, 4291) presented measurements of fluxes and spectra of atmospheric neutrons at different locations, altitude and weather conditions. Cattani et al. (SH 3.6, 4181) have shown that washing out of natural and cosmic ray induced radioactivity during rainout episodes results in enhanced radioactivity level as measured on the ground. Cattani et al. (SH 3.6, 4295) reported also measurements of γ-ray spectra at different atmospheric depths and locations. Environmental radioactivity measurements by SONTEL (Solar neutron telescope) at Gornergrat, Switzerland have been performed by Bütikofer et al. (SH 3.6, 4189) to show that count rates due to natural radon presence may mimic possible solar neutron signal.

6. Long-term cosmic ray intensity

Although cosmogenic isotopes serve as a proxy of cosmic ray intensity, it is not straightforward to reconstruct the flux of cosmic rays in the past from these data because of the complicated atmospheric transport of the isotopes before deposition. A model has been presented to calculate the expected cosmic ray flux for the last 400 years starting from solar activity (Usoskin et al., SH 3.4, 4041; Cini

Castagnoli et al., SH 3.4, 4045) using the following approach. Recently, Solanki et al. [28] developed a semi-empirical model to calculate the open solar magnetic flux from sunspot data (see Fig. 11.b). Bearing in mind that the open magnetic flux is directly related to the globally averaged IMF which, in turn, defines the long-term heliospheric modulation of cosmic rays, it can be converted to the so-called modulation potential Φ [15] (Fig. 11.c). This modulation potential has the meaning of the average rigidity loss of CR particles during their heliospheric transport and defines the differential spectrum of CR in the Earth's vicinity. Accordingly, CR flux is calculated since 1610 in terms of the standard polar neutron monitor count rate (Fig. 11.d) which agrees pretty well with the actual NM count rate for the last 50 years. Fig. 11.e presents a direct comparison of the calculated ^{10}Be production in polar atmosphere with the actual ^{10}Be measurements in Greenland [5] and in Antarctica [3]. A good agreement between the reconstructed and actual data over 400-year interval validates the applied model. Inverting the above model, Beer et al. (SH 3.5, 4147) estimated the long-term changes of the modulation strength on multi-millennium time scale from ^{10}Be data (Fig. 12.) depicting its high variability and recurrent occurrence of great minima as periods of reduced modulation.

6.1. Periods of unusual modulation

The level of heliospheric modulation strongly depends on energy/rigidity of cosmic rays, leading to quite a different level of modulation, e.g., for different neutron monitors: from few percent for equatorial up to 30 % for polar stations. It is also in the anti-phase relation to the solar cycle. However, during 1970s, the so-called mini-cycle in CR flux has occurred [36],[33],[34],[37], when the modulation was very unusual. It was rigidity independent, i.e. data from different CR detectors depicted the same degree of modulation in the broad range of CR rigidities (see, e.g., Fig. 2 in Ahluwalia SH 3.4, 4035 or Fig. 1 in Storini et al., SH 3.4, 4095). This episode forms a puzzle for the modulation theory. It can be related either to increased $\lambda_\perp$ or may appear due to an unusual heliospheric structure [4] or may imply an unaccounted mechanism like electric drift suggested by Ahluwalia (SH 3.4, 4035). It is also an open question if such a peculiarity is a repetitive feature (Storini et al., SH 3.4, 4095).

Using data from ionisation chamber measurements [24] as well as ^{10}Be content in Greenland ice, McCracken, Beer & McDonald (SH 3.4, 4031) and McCracken & Heikkila (SH 3.4, 4117) suggested that anomalously high flux of lower (<1 GeV) CR was registered during the 19 cycle minimum (1954–1955).

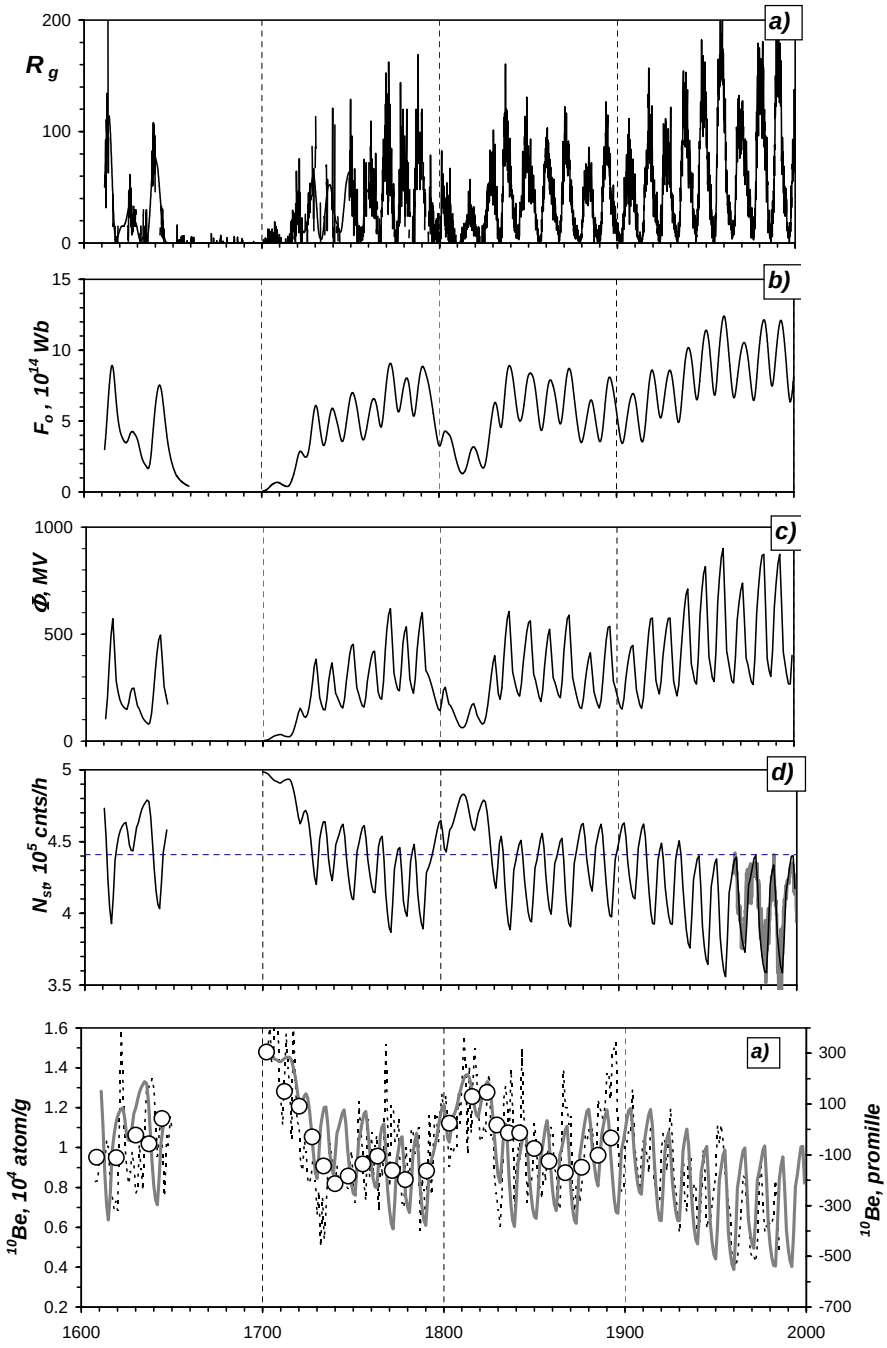

Fig. 11. Long-term cosmic ray reconstruction (from Usoskin et al., SH 3.4, 4041). a) Group sunspot numbers [18]; b) Calculated annual open solar magnetic flux [28]; c) Calculated modulation potential; d) Calculated (solid curve) and actually measured (grey curve) count rate of a polar neutron monitor; e) Calculated (grey curve) and actual annual ^{10}Be content in Greenland ice (dotted curve, [5]). Open circles represent the 8-year averaged ^{10}Be data from Antarctica [3].

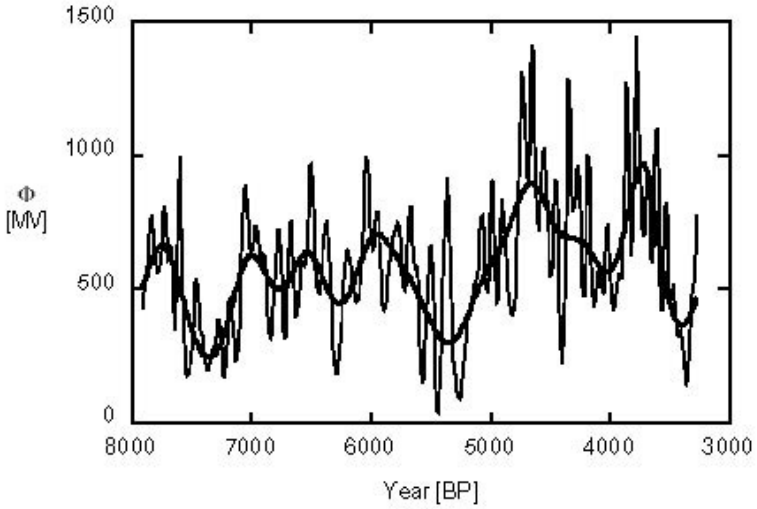

Fig. 12. Long-term reconstruction of the modulation strength from ^{10}Be data (from Beer et al., SH 3.5, 4147).

7. The Gnevyshev gap

The phenomenon of a dip in different solar cycle related indices around the very maximum of solar activity is called the Gnevyshev gap. Originally found in the large sunspots [16], it was later confirmed to exist in many other solar-related parameters [17],[29]. This effect is probably related to the global solar magnetic field reversal. Storini et al. (SH 3.4, 4049) presented an evaluation of the Gnevyshev gap effect in cosmic ray modulation as recorded by ground based instruments (neutron monitors and muon telescopes). They found that the Gnevyshev gap in the cosmic ray modulation has a strong rigidity dependence, i.e., it is decreasing towards higher energy/rigidity of cosmic ray particles (Fig. 13.).

Using a linear approximation (dotted line in the Figure), Storini et al. concluded that the Gnevyshev gap effect should not exist for cosmic rays above 150±20 GV. However, I would suggest to take into account a non-linear nature of the phenomena (see solid curve) which can lead to a possible effect even for higher energies. The results of the Sun's shadow investigation (see Section 4.) conducted by the Tibet collaboration (SH 3.4, 4061) show a clear Gnevyshev gap for 3 TeV cosmic rays (Fig. 14.). Although the shadow is not visible during the years 2000 and 2002 due to the strong scattering of 3 TeV particles by the solar magnetic field, the shadow is sharp in 2001, implying that the scattering was significantly reduced during the year of solar activity maximum. Accordingly, the Gnevyshev gap effect can influence even cosmic rays in TeV energy region.

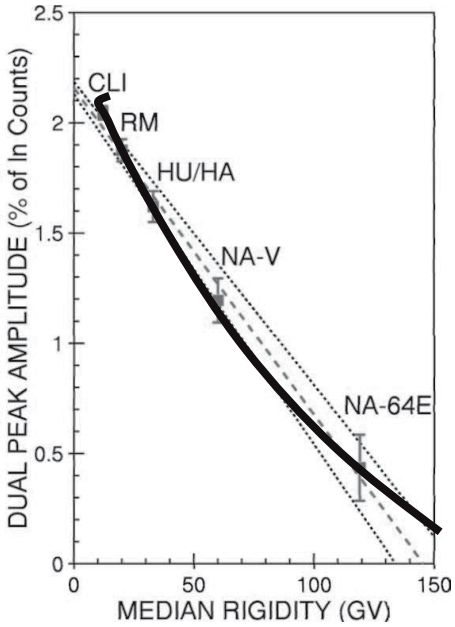

Fig. 13. The median rigidity dependence of the Gnevyshev gap effect in cosmic ray modulation (from Storini et al., SH 3.4, 4049). Dotted line presents a linear approximation of the effect, while the solid curve presents a non-linear effect suggested by the rapporteur. CLI, RM, HU/HA, and NA notations refer to Climax, Rome, Huancayo/Haleakala NMs and Nagoya muon telescope, respectively.

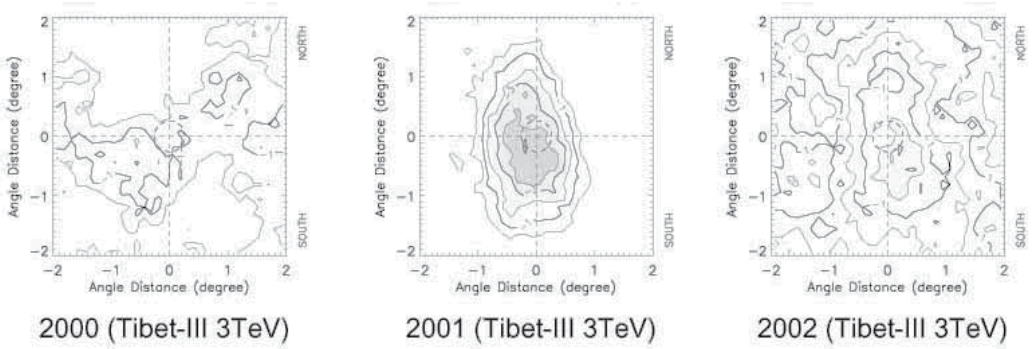

Fig. 14. The Sun's shadow in 3 TeV energy cosmic rays, as detected by the Tibet collaboration (SH 3.4, 4061).

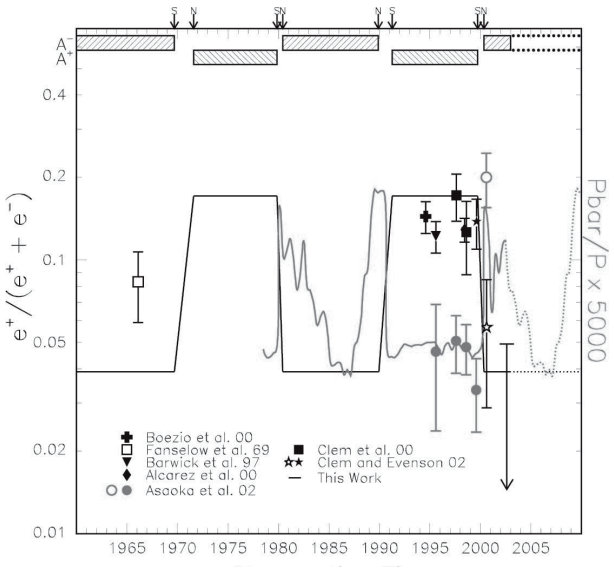

Fig. 15. Time profile of positron abundance (black) and antiproton-to-proton ratio (red) at a rigidity of 1.3 GV (from Clem & Evenson, SH 3.4, 4023). Solid symbols show data taken in the A+ state, while the open symbols represent data taken in the A- state.

8. 22-year cycle in CR modulation

The 22-year cycle in CR modulation is expected as a result of the CR partciles drift along the heliospheric current sheet (HCS). Since the direction of this drift depends on the product of IMF polarity and the particle's charge sign, it results in altering enhancements and reductions of the CR flux in the inner heliosphere near the ecliptic plane for the consecutive 11-year modulation cycles. This effect has been predicted theoretically already at the 16th ICRC in 1979 and supported by detailed model calculations (see, e.g., [19], [26]). Although this effect is clearly seen as the alteration of sharp and flat peaks in the neutron monitor count rates, more direct experimental evidences of this effect are of great interest. At this Conference, several new evidences of the 22-year cycle in CR modulation have been presented. Clem & Evenson (SH 3.4, 4023) presented a comprehensive analysis of available data on e^-/e^+ and antiproton-to-proton $\bar{p}/p$ ratios (Fig. 15.) and concluded that the results of measurements agree with the expected time profiles (solid lines). In particular, both e^-/e^+ and $\bar{p}/p$ ratios depict a simultaneous sharp jump in opposite directions that is concurrent with the global magnetic field reversal, implying significant and similar (but opposite) drift effect for both species with the charge of opposite sign. This work provides evidence for the HCS drift effect as dependent on both CR charge and IMF polarity. Further

evidences for the different CR modulation during odd and even-numbered cycles (i.e., studying only the IMF polarity effect) have been also presented (Ahluwalia, SH 3.4, 4035; Storini et al., SH 3.4, 4095; McCracken & Heikkila, SH 3.4, 4117). Dubey et al. (SH 3.4, 4091) reported on a shift of the diurnal anisotropy phase towards earlier hours during qA>0 cycles. Also the amplitude of 27-day CR variations was found to be different for odd- and even-cycles (Alania et al., SH 3.4, 4087). An interesting result was reported by Valdes-Galicia et al. (SH 3.4, 4053) on the alteration between 1.3- and 1.7-year periodicity in open/closed solar magnetic during odd-even cycles, implying a possible 22-year cycle in the solar magnetic flux.

9. Space weather

Space weather is related to variable radiation/magnetic conditions in the Earths environment, and several contributions broach this topic. Belov et al. (SH 3.6, 4213) studied a large statistics of satellite malfunctions (more than 6000 reported cases from about 300 satellites including the Soviet series of 50+ identical KOSMOS spacecrafts operating through years) in relation to different space weather parameters. Dividing all satellites in four different groups by their orbital parameters (altitude and inclination of the orbit), Belov et al. concluded that the most important factor responsible for the malfunctions is the fluence of low energy cosmic rays (both protons and electrons). They also promise to develop a method of short-term forecast of spacecraft malfunction warnings. Meanwhile, Dorman (SH 3.6, 4269) reviewed basic principles of space weather forecasting using CR data.

A rigorous study of the solar particle streaming around the Earth's magnetosphere has been performed by Kiraly (SH 3.5, 4057) using the long-lasting IMP-8 measurements and taking into account variable orbital parameters of the spacecraft. The directional distribution of the upstream particles was found to depend strongly on the solar cycle (see Fig. 16.).

Makhmutov et al. (SH 3.6, 4233) reviewed data of electron precipitation events recorded at a polar station during 1970-1987 and found a significant semi-annual variation. Considering different theories, the authors concluded that the Spring peak in electron precipitation is most likely related to Russel-McPherron effect while the Fall broad peak is probably a superposition of Russel-McPherron, Equinoctial and Axial effects.

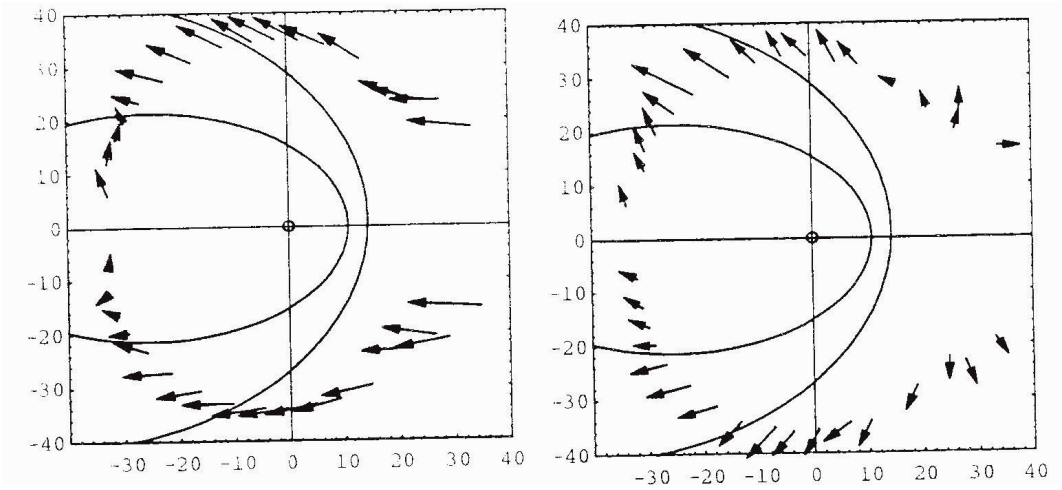

Fig. 16. Solar cycle dependence of energetic particle streaming (IMP-8 data): large variations of upstream ion anisotropy (from Kiraly, SH 3.4, 4057).

10. Geomagnetic rigidity cut-off

The geomagnetic field shields the Earth from charged particles, and this shielding changes with the (geomagnetic) latitude: from no shielding in polar caps where the magnetic lines are open to the very strong shielding in equatorial regions. The shielding is usually considered using a simplified term of the effective geomagnetic rigidity cut-off P_c so that CR particles with the rigidity below P_c cannot penetrate into the atmosphere at a given location. Changes of the geomagnetic field (orientation and strength of the dipole) are important for studies of CR on the long-term scale as they affect the cut-off rigidity. This issue has been considered by Smart & Shea (SH 3.6, 4201), Shea & Smart (SH 3.6, 4205) and Flückiger et al. (SH 3.6, 4229). Changes in the cut-off rigidity are very large in some regions (Fig. 17.) during the period of 1600–1900 and may reach up to 7 GV. The changes are significant even during the last century and should be carefully taken into account.

On the other hand, it is important to take into account the rapidly changing conditions of the dynamic magnetosphere when analyzing precise data from space borne instruments. At the Conference some results of detailed calculations of the geomagnetic cutoff for low-orbiting satellites have been presented by Smart et al. (SH 3.6, 4241), who succeeded reproducing the 1-min recorder radiation doses at a Space Shuttle flight, and by Desorgher et al. (SH 3.6, 4277).

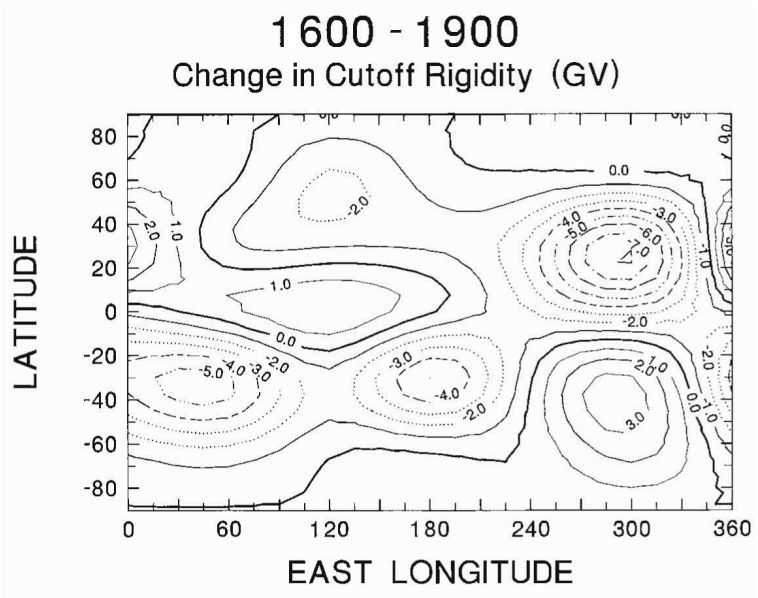

Fig. 17. Changes of the local geomagnetic rigidity cut-off between 1600 and 1900 (from Shea & Smart, SH 3.6, 4205).

11. Secondary particles

In nuclear interactions of CR with the Earths atmosphere, secondary particles can be produced. Depending on the energy and location, they can be magnetically trapped by the geomagnetic field and can be measured at low orbits. Authors of several contributions have studied this trapped population. Mikhailov et al. (SH 3.6, 4253) presented spectra of trapped light isotopes measured by the NINA-2 instrument during one year period 2000–2001 and concluded that rare light isotopes compose a distinct component of the Earth's inner radiation belts. Galper et al. (SH 3.6, 4257) presented a model to explain the observed light isotopes abundance. Miyasaka et al. (SH 3.6, 4265) calculated the flux of antiprotons produced locally in the residual atmosphere by GCR and concluded that such locally produced antiprotons (<1 GeV) should be several orders of magnitude more abundant at a low orbit than antiprotons of interstellar origin. A Monte-Carlo program has been presented by Zuccon et al. (SH 3.6, 4249) to calculate the radiation environment for low orbit satellites (below Van Allen belts).

Interesting result has been demonstrated by Nakagawa et al. (SH 3.6, 4261) who found, using an X- and γ-ray instrument onboard HETE-2 satellite, an unusual time-variable increase of low energy electrons near the South Atlantic anomaly. This increase has a steep energy spectrum and appear during/after major geomagnetic storms.

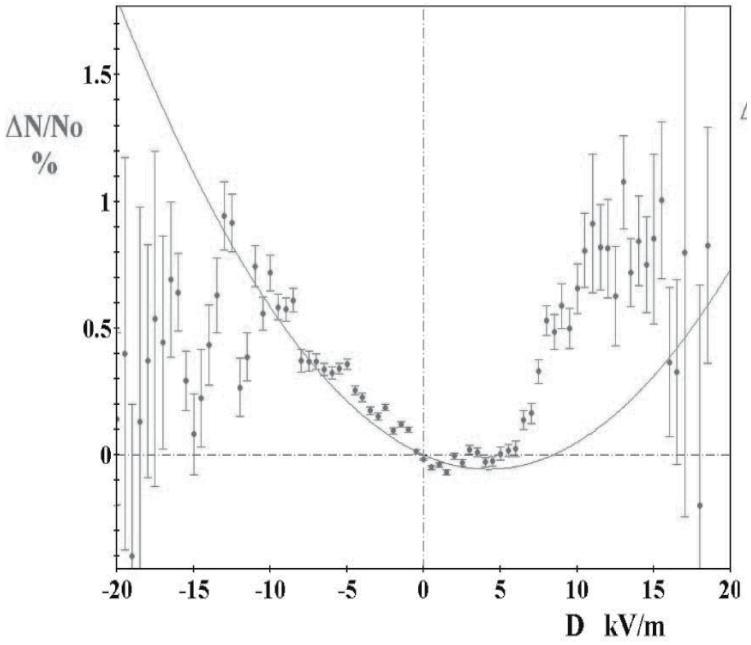

Fig. 18. The regression of the soft component intensity vs. the corrected electric field measured at the Baksan observatory (from Khaerdinov et al., SH 3.6, 4165).

12. Cosmic Rays and thunder clouds

A particular interest is growing to the (secondary) particles acceleration by the electric field during thunderstorms. Two groups presented their results. The Mt. Norikura group (Muraki et al., SH 3.6, 4177) preseneted evidence for proton acceleration by electric field in thunder clouds that was supported by the Monte-Carlo simulations. The 26-day recurrence of such events is also found relating them to the solar rotational period. The Baksan group (Khaerdinov et al., SH 3.6, 4165; SH 3.6, 4169) performed a rigorous regression analysis of soft (electron) and hard (muon) components variations in relation with the electric field. They have analyzed 88 events during 2000–2002 (Fig. 18.) and found the expected parabolic shape (cf. Fig. 3 in Muraki et al., SH 3.6, 4177). The bump in the electron intensity clearly visible in the right hand side of Fig. 18. is interpreted as a signature of electron acceleration (runaway electrons) at higher level (see also Muraki et al. SH 3.6, 4177) around the time of lightning. This is consistent with the idea of runaway electrons driving the lightning channel. Note that the sign of the electric field measured in Mt. Norikura is incorrect in the published ICRC proceeding (Muraki et al., SH 3.6, 4177) and should be inverted (Y. Muraki, personal communication). After this correction, all presented results are consistent with each other (including

also those discussed during the 27th ICRC). Ermakov and Stozhkov (SH 3.6, 4157) described a qualitative generic model of the CR role in thunder cloud production. According to this model, CR provide the necessary number of ions in the lower atmosphere as well as channels for the lightning discharge.

13. Miscellanious

This section briefly discusses the results which do not fit directly the above sections. Humble and Duldig (SH 3.6, 4197) studied asymptotic directions of a neutron monitor in the dynamical megnetospheric model. Notable daily and seasonal variations of the viewing directions, which are not expected in the usual static models, were found up to 7 GV of CR rigidity. This earlier unaccounted effects may lead to a partly spurious sederial anisotropy.

Alania et al. (SH 3.6, 4087) solved the Parker's equation of cosmic ray heliospheric transport in terms of the generalized 3D anisotropic diffusion tensor (see [1] for notations):

$$\begin{aligned}
\kappa_{11} &= \kappa_0 \left[\cos^2\gamma\cos^2\psi + \alpha\left(\cos^2\gamma\sin^2\psi + \sin^2\gamma\right)\right] \\
\kappa_{12} &= \kappa_0 \left[\sin\gamma\cos\gamma\cos^2\psi\,(1-\alpha) - \alpha_1\sin\psi\right] \\
\kappa_{13} &= \kappa_0 \left[\sin\psi\cos\gamma\cos\psi\,(\alpha-1) - \alpha_1\sin\gamma\cos\psi\right] \\
\kappa_{21} &= \kappa_0 \left[\sin\gamma\cos\gamma\cos^2\psi\,(1-\alpha) + \alpha_1\sin\psi\right] \\
\kappa_{22} &= \kappa_0 \left[\sin^2\gamma\cos^2\psi + \alpha\left(\sin^2\gamma\sin^2\psi + \cos^2\gamma\right)\right] \\
\kappa_{23} &= \kappa_0 \left[\sin\gamma\sin\psi\cos\psi\,(\alpha-1) + \alpha_1\cos\gamma\cos\psi\right] \\
\kappa_{31} &= \kappa_0 \left[\cos\gamma\sin\psi\cos\psi\,(\alpha-1) + \alpha_1\sin\gamma\cos\psi\right] \\
\kappa_{32} &= \kappa_0 \left[\sin\gamma\sin\psi\cos\psi\,(\alpha-1) - \alpha_1\cos\gamma\cos\psi\right] \\
\kappa_{33} &= \kappa_0 \left[\sin^2\psi + \alpha\cos^2\psi\right]
\end{aligned} \tag{1}$$

They found that the 27-day variations of (> 10 GV) GCR are greater during the qA>0 than during qA<0 cycles which is ascribed to the involution of the oppositely directed drift streams of GCR in the convection by the solar wind possessing the heliolongitudinally asymmetric velocity.

Some results on observations of light flashes in the astronaut's eyes onboard MIR and ISSI associated with energetic particles have been presented by the Sileye collaboration (SH 3.6, 4161; SH 3.6, 4125). Although the experiment itself is focused on astrobiology rather than on cosmic rays, they can measure, using the auxiliary equipment, the nuclear composition of cosmic rays inside the space stations.

Quite unusual index of solar activity/cosmic ray intensity in the Medieval times has been suggested by Pustilnik et al. (SH 3.5, 4131): the wheat price in

England. Due to the closed market and the risky agriculture region the wheat market had highly nonlinear response to meteorological conditions. The wheat prices show a good agreement with the cosmogenic isotopes in earlier times supporting this idea.

14. Highlights

Many interesting results have been presented at the 28th ICRC covering a broad field related to cosmic rays. The most interesting (subjectively selected) new results in the Sessions reviewed here (SH 3.4–3.6) have been obtained in the following fields (in no particular order).

- New measurements of cosmogenic isotopes. In particular, the new high precision ^{14}C annual data have been presented covering the Maunder and, for the first time, Spörer minima of solar activity.
- Environmental monitoring.
- Charged particle acceleration during thunderstorms.
- Study of long-term geomagnetic cut-off rigidities.
- Measurements and models for trapped particles.

Acknowledgements

I am grateful to the Organizing Committee of the Conference for inviting me and giving an opportunity to present this review. I thank many conferees from whom I learned a lot during the "corridor discussions," in addition to the formal presentations. Special thanks to Harjit Ahluwalia, Michael Alania, Jürg Beer, Giuliana Cini Castagnoli, Lev Dorman, Marc Duldig, John Humble, Karel Kudela, Alexander Lidvansky, Ken McCracken, Hiroko Miyahara, Harm Moraal, Yasushi Muraki, Lev Pustil'nik, Oscar Saavedra, Peggy Shea, Don Smart, Marisa Storini, Yuri Stozhkov, Jose Valdec-Galicia.

References

[1] Alania, M. V., 2002, Acta Phys. Polonica B, 33, 1149

[2] Allen, D. J. et al. 2003, J. Geophys. Res., 108 (D4), TOP 3-1, DOI 10.1029/2001JD001428

[3] Bard, E., G. M. Raisbek, F. Yiou, & J. Jouzel 1997, Earth Planet. Sci. Lett., 150, 453

[4] Benevolenskaya, E. E. 1998, Solar Phys., 181, 479

[5] Beer, J. et al. 1990, Nature, 347, 164

[6] Beer, J., S. Tobias, & N. Weiss 1998, Solar Phys., 181, 237

[8] Castagnoli, G., & D. Lal 1980, Radiocarbon, 22 (2), 133

[9] Dibb, J. E. 1989, J. Geophys. Res., 94, 2262

[10] McCracken, K. G., Beer, J., & McDonald, F. B. 2002, Geophys. Res. Lett., 29(24), 2161

[11] Cliver, E. W., V. Boriakoff, & K. H. Bounar 1998, Geophys. Res. Lett., 25, 897

[12] Damon, P. E., C. J. Eastoe, & I. B. Mikheeva 1999, Radiocarbon, 41, 47

[13] Gladysheva, O. G., & G. A. M. Dreschhoff 1997, Izvestiya RAN, ser. fiz., 61, 1062 (in Russian).

[14] Gladysheva, O. G., G. E. Kocharov, G. A. Kovaltsov, I. G. Usoskin 2002, Adv. Space Res., 29, 1707

[15] Gleeson, L. J. & W. I. Axford 1968, Astrophys. J., 154, 1011

[16] Gnevyshev, M. N. 1967, Sol. Phys., 1, 107

[17] Gnevyshev, M. N. 1977, Sol. Phys., 51, 175

[18] Hoyt, D. V. & K. Schatten 1998, Solar Phys. 179, 189

[19] Jokipii, R. & B. Thomas 1981, Astrophys. J., 243, 1115

[20] Kocharov, G. E., V. M. Ostryakov, A. N. Peristykh, V. A. Vasil'ev 1995, Solar Phys., 159, 381

[21] Křivský, L., & K. Pejml 1988, Astron. Inst. Czech. Acad. Sci, 75, 32

[22] Masarik, J., & J. Beer 1999 J. Geophys. Res., 104 (D10), 12099

[23] McCracken, K. G. et al. 2001a, J. Geophys. Res., 106, 21, 585

[24] Neher, H. V. 1967, J. Geophys. Res., 72, 1527

[25] Peristykh, A. N., & P. E. Damon 1998, Solar Phys., 177, 343

[26] Potgieter, M., & H. Moraal 1985, Astrophys. J., 294, 425

[27] Silverman, S. M. 1992, Rev. Geophys., 30, 4, 333

[28] Solanki, S. K., M. Schüssler & M. Fligge 2000, Nature, 408, 445

[29] Storini, M., S. Pase, J. Sykora, M. Parisi 1997, Sol. Phys., 172, 317

[30] Stuiver, M. & T. F. Braziunas 1993, Holocene, 3, 289

[31] Stuiver, M. & T. F. Braziunas 1998, Geophys. Res. Lett., 25, 329

[32] Suess, H. E. 1955, Science, 122, 415

[33] Usoskin, I. G. et al. 1997, in: Proc. 25th Intern. Cosmic Ray Conf., Durban, 1997, v. 2, 201

[34] Usoskin, I. G. et al. 1998, J. Geophys. Res., 103 (A5), 9567

[35] Usoskin, I. G., K. Mursula, & G. A. Kovaltsov 2001, J. Geophys. Res., 106(A8), 16039

[36] Webber, W. R., & J. A. Lockwood 1988, J. Geophys. Res., 93 (8), 8735

[37] Wibberenz, G., I. G. Richardson & H. V. Cane 2002, J. Geophys. Res., 107(A11), SSH 5-1, DOI 10.1029/2002JA009461

[38] Zeller, E. J., & B. C. Parker 1981, Geoph. Res. Lett., 8, 895